



Article

Synthesis and Characterization of Free-Stand Graphene/Silver Nanowire/Graphene Nano Composite as Transparent Conductive Film with Enhanced Stiffness

Chuanrui Guo *D, Yanxiao Li, Yanping Zhu, Chenglin WuD and Genda ChenD

Department of Civil, Architectural and Environmental Engineering, Missouri University of Science and Technology, Rolla, MO 65401, USA; yl42y@mst.edu (Y.L.); yz6d7@mst.edu (Y.Z.); wuch@mst.edu (C.W.); gchen@mst.edu (G.C.)

* Correspondence: cggfb@mst.edu

Received: 19 June 2020; Accepted: 11 July 2020; Published: 13 July 2020



Featured Application: In this work, free-stand Gr/AgNW/Gr nanocomposite has been synthesized and characterized for interfacial bonding study, ultrasensitive sensor, and actuator application.

Abstract: As-grown graphene via chemical vapor deposition (CVD) has potential defects, cracks, and disordered grain boundaries induced by the synthesis and transfer process. Graphene/silver nanowire/graphene (Gr/AgNW/Gr) sandwich composite has been proposed to overcome these drawbacks significantly as the AgNW network can provide extra connections on graphene layers to enhance the stiffness and electrical conductivity. However, the existing substrate (polyethylene terephthalate (PET), glass, silicon, and so on) for composite production limits its application and mechanics behavior study. In this work, a vacuum annealing method is proposed and validated to synthesize the free-stand Gr/AgNW/Gr nanocomposite film on transmission electron microscopy (TEM) grids. AgNW average spacing, optical transmittance, and electrical conductivity are characterized and correlated with different AgNW concentrations. Atomic force microscope (AFM) indentation on the free-stand composite indicates that the AgNW network can increase the composite film stiffness by approximately 460% with the AgNW concentration higher than 0.6 mg/mL. Raman spectroscopy shows the existence of a graphene layer and the disturbance of the AgNW network. The proposed method provides a robust way to synthesize free-stand Gr/AgNW/Gr nanocomposite and the characterization results can be utilized to optimize the nanocomposite design for future applications.

Keywords: graphene; silver nanowire; nano composite; synthesis; characterization

1. Introduction

Graphene, a two-dimensional material consisting of single layer carbon atoms in hexagonal lattice, has attracted much attention since Geim et al. [1,2] first produced it from graphite in a lab through the mechanical exfoliation method. Thanks to its excellent optical, electrical, mechanical, and thermal properties, graphene is an ideal material for many applications such as flexible touchscreen, organic light emitting diode (OLED), chemical sensor, and biological devices [3–7]. In order to achieve industry-scale production, various graphene synthesis methods were developed by researchers [8–12]. Among them, the chemical vapor deposition (CVD) technique is most effective owing to its robust capability of large area monolayer graphene production [9,13]. However, as-grown graphene film on metal catalyst (Cu, Ni) through the CVD process has intrinsic disorders at grain boundaries induced

Appl. Sci. 2020, 10, 4802 2 of 12

by the metal recrystallization under high temperature (>1000 $^{\circ}$ C) [14]. In addition, the transfer process via polymer thin film and etching will introduce defects, cracks, and wrinkles on the graphene layer [9,15–17]. These drawbacks will reduce the electrical conductivity and mechanical strength of the as-grown graphene. Recently, a silver nanowire (AgNW) network has been embedded between two graphene layers to form a Gr/AgNW/Gr sandwich-structure composite [3,6,18–20]. The proposed composite has excellent electrical conductivity and optical transmittance. In particular, the electrical conductivity remains stable after more than 20,000 bending cycles [18], which indicates its robust mechanical strength and flexibility. Moreover, the two graphene layers encapsulation can prevent AgNW from oxidization, thus the composite has a long-term stability of performance.

Although the Gr/AgNW/Gr composite shows excellent properties, there are three main technical challenges that limit its broader applications: (1) the bottom substrate (silicon, PET, glass, and so on) for composite synthesis reduces the optical transmittance, electrical conductivity, and mechanical flexibility. For applications such as battery, transparent electrode, and biological devices, free stand Gr/AgNW/Gr film is essential to achieve the required functions. (2) Interfacial bonding mechanism between AgNW and graphene layers is unknown, which is critical for the mechanics model and performance analysis. (3) Correlation between the composite properties and AgNW concentrations has not been studied, which is necessary for the optimization of the structure design.

In this paper, a vacuum annealing method is proposed for the first time to synthesize free-stand two-layer graphene and Gr/AgNW/Gr composite on TEM grids. AgNW concentrations varying from 0.2 to 1.0 mg/mL are added for the nanocomposite to study the concentration effect. The average spacing of the AgNW network is measured first through scanning electron microscope (SEM) images and its correlation with concentration is then established. Optical transmittance at 550 nm and sheet resistance of the composite are characterized and compared with the two-layer graphene. Atomic force microscope (AFM) indentation is conducted and the stiffness of both the two-layer graphene and composites with different AgNW concentrations is obtained and compared from the force—displacement curve. Raman spectroscopy is conducted to prove the graphene existence and the disturbance of the AgNW network. The characterization results can be utilized for nanocomposite design and interfacial bonding study between the AgNW and graphene layer.

2. Materials and Methods

2.1. Synthesis of Free-Stand Two-Layer Graphene and Gr/AgNW/Gr Nanocomposite

Figure 1 shows the low preassure chemical vapor deposition (LPCVD) system for graphene synthesis. The mass flow controller (MFC) controls the quantity of gas that flows into the quartz tube for reaction. A 125 μ m thick copper foil (99.9%, Alfa Aesar 13380, Alfa Aesar, Ward Hill, MA, USA) was pretreated in acetic acid (99.7%, Sigma Aldrich 695092, Sigma Aldrich, St Louis, MO, USA) for 48 h and then cleaned with DI water, IPA and acetone. Monolayer graphene was synthesized on the copper foil in the reaction chamber (quartz tube) with 5 sccm (standard cubic centimeter per minute) hydrogen flow for 30 min and then 5 sccm methane flow for 10 min under 1030 °C at ~100 mTorr vacuum pressure. The as-grown graphene on copper was then cooled down to room temperature for next step usage.

Appl. Sci. 2020, 10, 4802 3 of 12

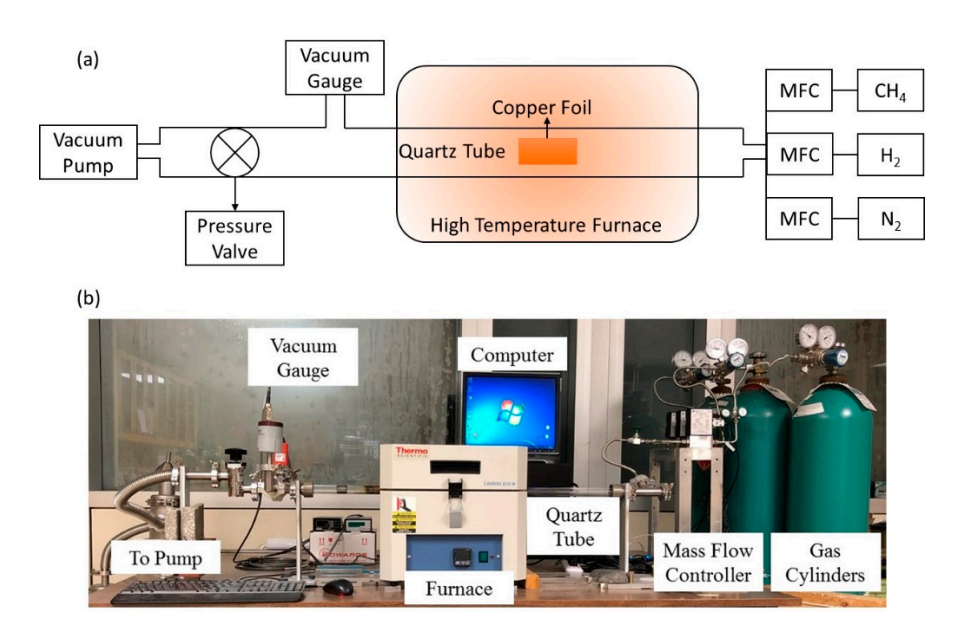


Figure 1. (a) Schematic illustration and (b) setup of the low pressure chemical vapor deposition (LPCVD) system. MFC, mass flow controller.

Figure 2 shows the procedure of free-stand two-layer graphene and Gr/AgNW/Gr nanocomposite synthesis process. As-grown graphene on copper was spin coated with Poly (methyl methacrylate) (PMMA, Sigma Aldrich 182265, $M_W = 996,000$) in chlorobenzene (46mg/mL) solution at 4000 RPM for 30 s. The PMMA/Gr/copper was heated under 170 °C for 10 min to evaporate the chlorobenzene solvent and then floated on the copper etchant (Sigma Aldrich 667528) for 2 h to dissolve the copper substrate. The floated PMMA/Gr film was cleaned with deionized (DI) water twice and flipped over to make the graphene layer on the top. The Gr/PMMA film was transferred on a square meshed TEM grid (EMS 400-Ni, hole size 50 µm). A 3 µL solution of AgNW dispersed in isopropyl alcohol (IPA) (ACS Materials, Agnw-L100, diameter = 30 nm, length = $100 \sim 150 \mu m$) with five different concentrations (0.2, 0.4, 0.6, 0.8, and 1.0 mg/mL) was applied on the Gr/PMMA surface through a micro syringe with needle. After the IPA dried at room temperature, another top layer PMMA/Gr film was transferred onto the AgNW/Gr/PMMA sample. The Gr/AgNW/Gr composite was free-standed on the TEM grid after a 30 min annealing process in vacuum (~50 mTorr) at 380 °C to evaporate the PMMA film. For comparison, a two-layer free-stand graphene film was also prepared by the similar procedures without applying the AgNW. The average thickness of the Gr/AgNW/Gr nanocomposite is ~31 nm based on the diameter of the AgNW (30 nm) and thickness of monolayer graphene (0.335 nm).

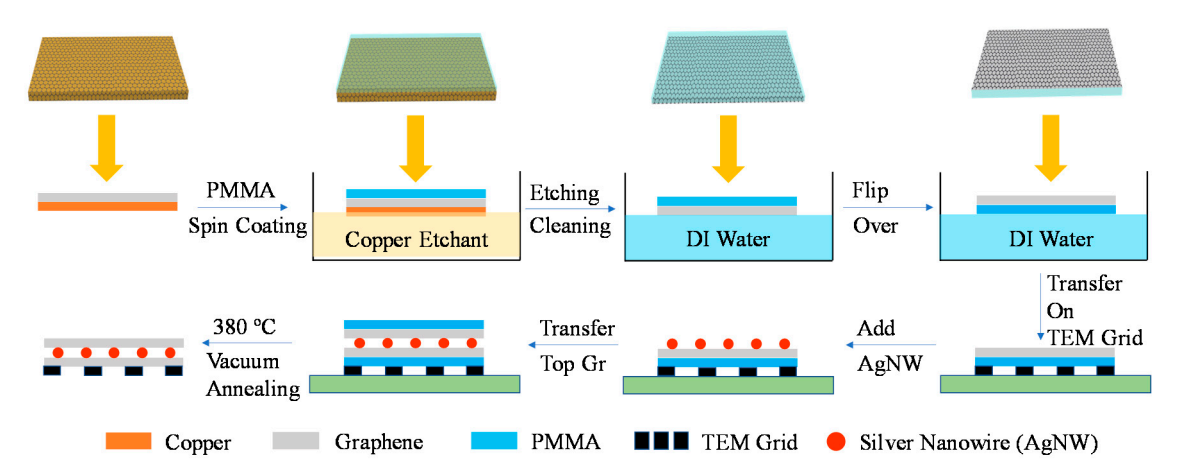


Figure 2. Schematic procedures of free-stand Gr/AgNW/Gr composite. PMMA, poly (methyl methacrylate).

Appl. Sci. 2020, 10, 4802 4 of 12

2.2. Optical Transmittance Characterization

The optical transmittance of a bare glass slide was first characterized through the optic transmittance meter (WTM-1100) at 550 nm as baseline. Monolayer and bilayer graphene and the Gr/AgNW/Gr with different AgNW concentrations were transferred on the slides independently and characterized by the meter. The measured values were divided by the baseline value to get the characterized transmittance accordingly.

As shown in Figure 3, a three-layer thin film model is introduced to characterize the optical transmittance of the composite. The wavelength of the light source is 550 nm, which is far greater than the AgNW diameter (~ 30 nm). Therefore, the diffraction effect on AgNW and interference between two graphene layers are neglected. The total optical transmittance T can be expressed as follows:

$$T = \frac{I}{I_0} = T_G \cdot T_A \cdot T_G \tag{1}$$

where T_G is the transmittance of graphene layer. For monolayer graphene, T_G is 97%, while for two-layer graphene, the value drops to 93%. T_A is the transmittance of the AgNW network, which varies with concentrations. T_A values with five concentrations were measured first and then the total optical transmittance could be calculated using Equation (1).

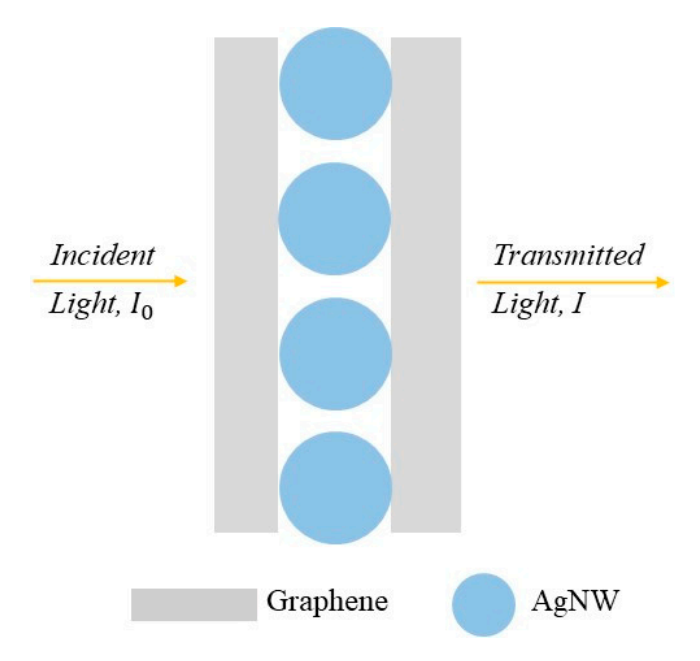


Figure 3. Three-layer thin film model of the nanocomposite.

2.3. Sheet Resistance Characterization

The sheet resistance was characterized using the Van der Pauw (four-point method) measurement [9], as shown in Figure 4. Four copper foil (25 μ m thick) electrodes were connected to each corner of the sample. A direct current (DC) was applied on two adjacent points and the voltage between the other two points was measured. The sheet resistance was then calculated as follows:

$$R_{\rm S} = \frac{\pi}{\ln 2} \frac{V}{I} = 4.53 \frac{V}{I} \tag{2}$$

Appl. Sci. 2020, 10, 4802 5 of 12

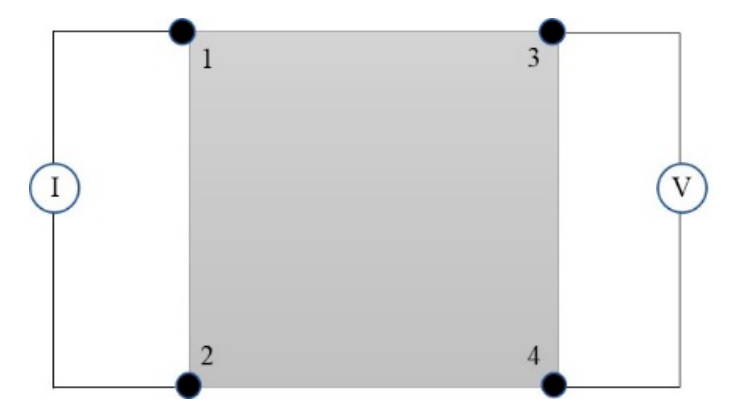


Figure 4. Schematic view of the Van der Pauw measurement.

Multiple measurements were conducted and averaged to obtain the sheet resistance value.

Sheet resistance of the composite R_S is determined by three components: sheet resistance of the graphene layer R_G and AgNW network R_A , and contact resistance R_C between the first two components. As shown in Figure 5, three types of contact conditions and corresponding circuit models are defined based on the contact condition. The fully contact model is an assumed ideal condition in which the AgNW-to-graphene and graphene-to-graphene are in perfect adhesion with no contact resistance. The no contact model is another assumed condition in which AgNW and graphene layers have no contact with each other. These two assumptions are set to capture the upper and lower bond of the actual sheet resistance of the nanocomposite, which is described by the actual contact model. Sheet resistances of these three conditions can be expressed as follows:

$$R_N = R_A \tag{3}$$

$$R_S = \frac{R_G^2(R_A + R_C) + R_C R_G (2R_A + R_C)}{2R_A (R_C + R_G) + (R_C + R_G)^2}$$
(4)

$$R_F = \frac{R_G R_A}{2R_A + R_G} \tag{5}$$

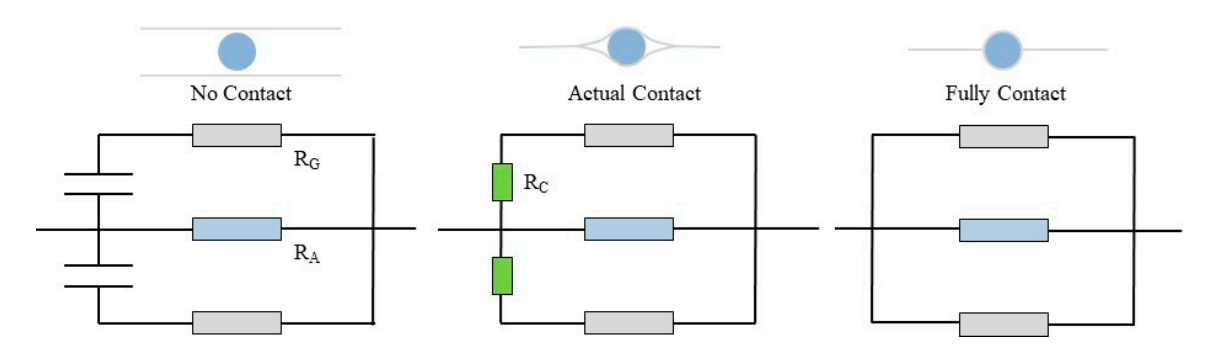


Figure 5. Circuit models of the composite sheet resistance.

For monolayer graphene synthesized by the LPCVD method, the measured sheet resistance R_G is approximately 275 Ω/\Box . The AgNW sheet resistance R_A was measured with different concentrations first using the four-point method. The sheet resistances of no contact and fully contact conditions can be calculated using Equations (3) and (5). The actual sheet resistances of the composite were then measured and compared with various AgNW concentrations.

Appl. Sci. 2020, 10, 4802 6 of 12

2.4. Atomic Force Microscopy

The stiffness of the nanocomposite was characterized by the atomic force microscope (AFM) indentation. As shown in Figure 6a, the AFM consists of a cantilever probe, photo diode, and laser. The laser and diode are used to measure the displacement of the probe. The cantilever probe is designed to measure the force. Figure 6b,c shows the probe tip after indentation, which has the residual graphene and nanocomposite on it.

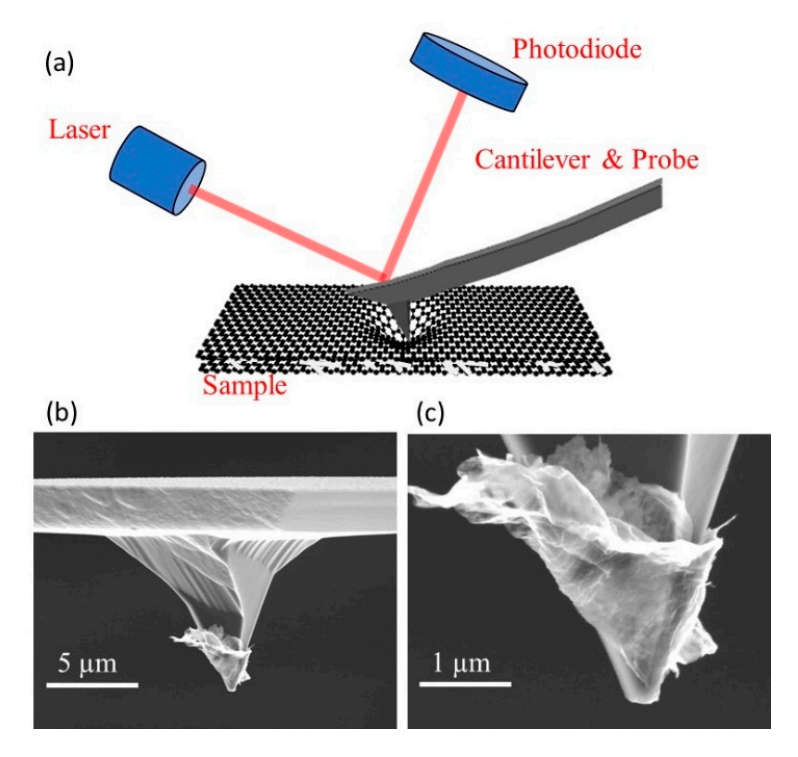


Figure 6. (a) Schematic illustration of the atomic force microscope (AFM) and (b,c) zoom in images of the AFM tip after indentation.

3. Results and Discussion

3.1. Silver Nanowire Average Spacing

Figure 7 shows the optical microscope images of the two-layer graphene and the Gr/AgNW/Gr nanocomposite (higher illumination to emphasize the AgNW). Some ruptured holes can be observed on the grid owing to the synthesis process. Figure 8 shows the SEM images of two-layer graphene and Gr/AgNW/Gr composites with different AgNW concentrations. As the nanowire is randomly distributed between two graphene layers, average AgNW spacing is first characterized. Multiple measurements of the AgNW spacing were conducted and averaged to obtain the average spacing value. As shown in Figure 9, the average spacing decreases linearly from 4.2 μ m to 1.5 μ m with the increased AgNW concentrations.

Appl. Sci. 2020, 10, 4802 7 of 12

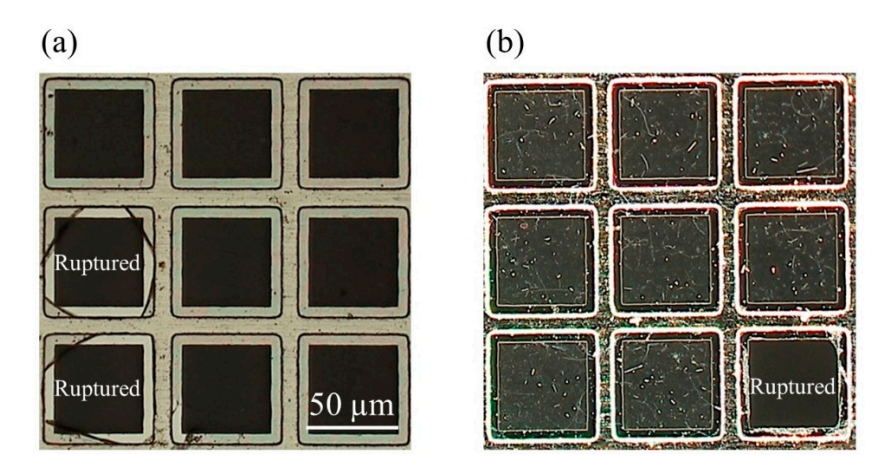


Figure 7. Optical microscope images of (a) two-layer graphene and (b) Gr/AgNW/Gr nanocomposite.

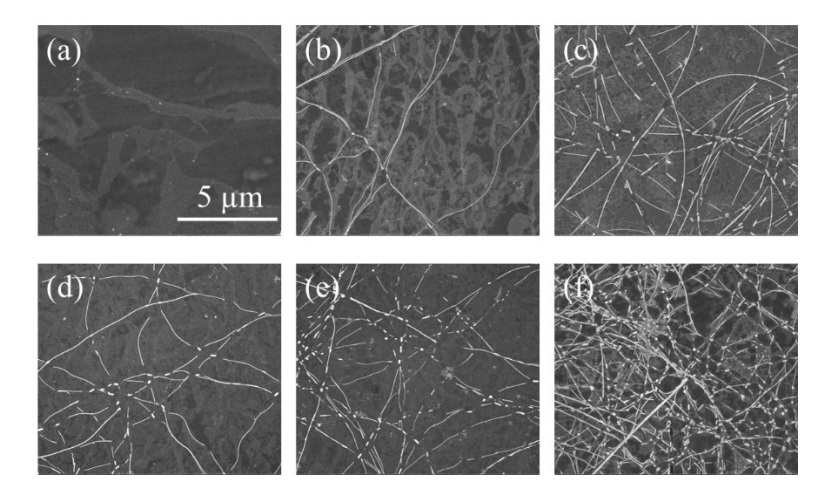


Figure 8. SEM images of (a) two-layer graphene; (b–f): Gr/AgNW/Gr composite with AgNW concentration of 0.2, 0.4, 0.6, 0.8, and 1.0 mg/mL.

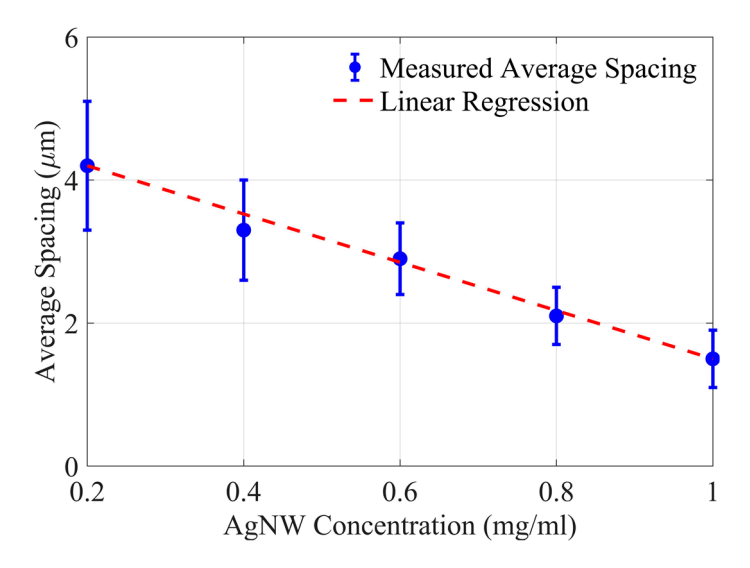


Figure 9. AgNW network average spacing with different concentrations.

3.2. Optical Transmittance

Table 1 lists the transmittance of the AgNW network, as well as calculated and measured values of the composite with five different AgNW concentrations. All the values decrease with the increasing

Appl. Sci. 2020, 10, 4802 8 of 12

AgNW concentrations because a larger quantity of AgNW will block more light. It can also be seen that the proposed model fits the measured value well with a maximum error of 6%.

| Table 1. | Comparison of the measur | ed and calculated transr | mittance values with different A | gNW |
|----------|--------------------------|--------------------------|----------------------------------|-----|
| concenti | ations. | | | |

| AgNW Concentration (mg/mL) | AgNW Transmittance (Measured) | Gr/AgNW/Gr Transmittance (Calculated) | Gr/AgNW/Gr Transmittance (Measured) | Error |
|----------------------------------|-------------------------------------|---|---|-------|
| 0.2 | 87.7% | 81.6% | 85.7% | 5% |
| 0.4 | 86.6% | 80.5% | 81.4% | 1% |
| 0.6 | 85.0% | 79.1% | 80.6% | 2% |
| 0.8 | 83.5% | 77.6% | 80.1% | 3% |
| 1.0 | 79.3% | 73.7% | 78.3% | 6% |

3.3. Sheet Resistance

Figure 10a shows the measured actual sheet resistance of the composite together with the calculated no contact, fully contact resistances. It is obvious that the measured sheet resistance of the composite locates between the upper and lower values calculated from the no contact and fully contact models. Therefore, the actual contact model is assumed to represent the average contact condition of the Gr/AgNW/Gr composite well.

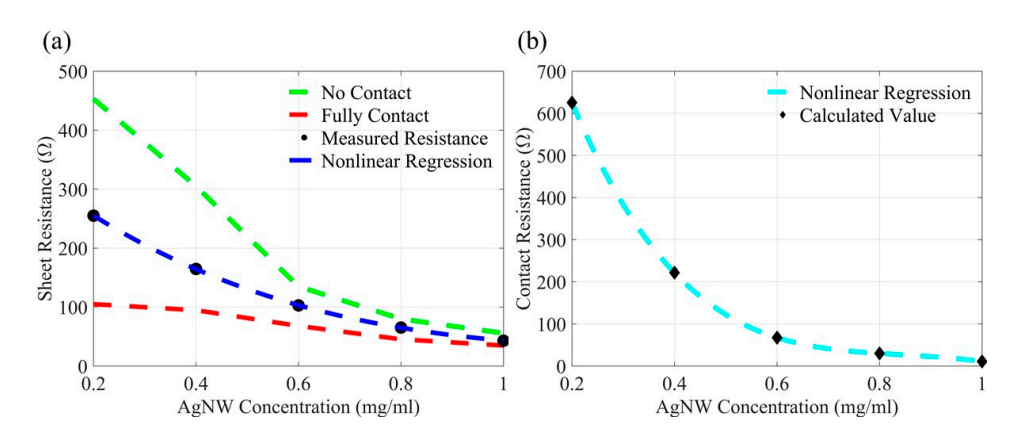


Figure 10. (a) Sheet and (b) contact resistance with different AgNW concentrations.

On the basis of Equation (3) and the measured sheet resistance of the composite, contact resistances with different AgNW concentrations can be derived and are shown in Figure 10b. Nonlinear regression of the sheet resistance R_S and contact resistance R_C is conducted and the correlation functions with various AgNW concentrations ϕ are obtained as follows:

$$R_S = -137.5\phi^3 + 534.3\phi^2 - 735.6\phi + 382, R^2 = 0.98$$
 (6)

$$R_C = -2410\phi^3 + 5920\phi^2 - 4883.8\phi + 1384.2, R^2 = 0.96$$
 (7)

The measured sheet resistance of the AgNW network, Gr/AgNW/Gr nanocomposite, and calculated contact resistance value with five AgNW concentrations is listed in Table 2. It can be seen that all the values decrease with the increased AgNW concentrations. This is because the AgNW network with a higher concentration has more connection joints within the network and a greater connection area with the two graphene layers that can increase the conductivity.

Appl. Sci. 2020, 10, 4802 9 of 12

| AgNW Concentration (mg/mL) | AgNW Sheet Resistance Ω/□ | Gr/AgNW/Gr Sheet Resistance (measured) Ω/□ | Contact Resistance Ω/□ |
|-------------------------------|---------------------------------|--|------------------------------|
| 0.2 | 453 | 255.1 | 625.5 |
| 0.4 | 305 | 164.7 | 221.7 |
| 0.6 | 135 | 102.9 | 67.6 |
| 0.8 | 79.9 | 65.3 | 30.1 |
| 1.0 | 55.8 | 43.1 | 10.9 |

Table 2. Comparison of sheet resistances with different AgNW concentrations.

3.4. Atomic Force Microscope Indentation

Table 3 and Figure 11a show the stiffness values and the force—displacement curves of the AFM indentation on the free-stand two-layer graphene and Gr/AgNW/Gr composites. Figure 11b,c shows the SEM images of the two-layer graphene and the Gr/AgNW/Gr nanocomposite after the AFM indentation. The cut-wire phenomenon observed on the nanocomposite indicates the strengthening effect of the AgNW on increasing the mechanical property of the nanocomposite. Compared with two-layer graphene, the stiffness of the composite increases with higher AgNW concentrations, while it becomes stable after 0.6 mg/mL with the value of around 2150 N/m, which indicates the maximum stiffness enhancement by the AgNW network reaches 0.6 mg/mL. This is owing to the limited interfacial bonding strength between the graphene layer and the AgNW network. When the AgNW concentration is higher than 0.6 mg/mL, the interfacial bonding between the Gr and AgNW dominates the stiffness of the nanocomposite. Therefore, the continuously increased AgNW concentration after 0.6 mg/mL cannot enhance the mechanical strength of the nanocomposite.

Table 3. Stiffness values under different concentrations.

| Concentration (mg/mL) | 0 | 0.2 | 0.4 | 0.6 | 0.8 | 1 |
|-----------------------|--------|--------|---------|---------|---------|---------|
| Stiffness (N/m) | 468.75 | 716.54 | 1201.88 | 2165.71 | 2135.11 | 2157.06 |

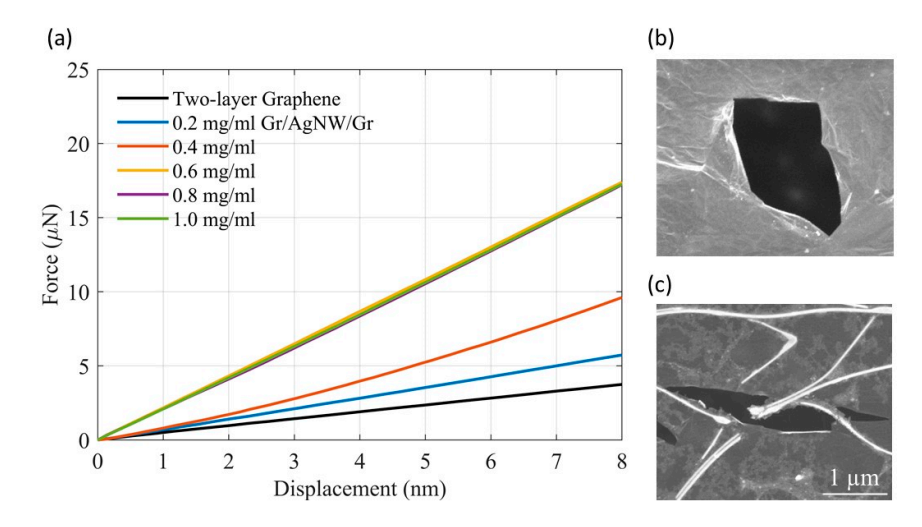


Figure 11. (a) Force–displacement curves of two-layer graphene and Gr/AgNW/Gr composite. SEM images of (b) two-layer graphene and (c) Gr/AgNW/Gr nanocomposites after AFM indentation.

3.5. Raman Spectroscopy

Figure 12 shows the Raman spectra of two-layer graphene and the Gr/AgNW/Gr composite. Raman shift at D, G, D', and 2D peaks and intensity ratio of I_G/I_{2D} are listed in Table 4. The higher intensity at D peak in the composite spectra indicates that the AgNW between two graphene layers increases the disorder level of the sp^2 hybridization. Besides, the localized vibration mode of AgNW

Appl. Sci. 2020, 10, 4802

splits the D' peak from the original G peak. The I_G/I_{2D} ratio is commonly used to determine the number of graphene layers [9,16,21–23]. As both samples have two layers of graphene, the ratio values are close to each other. The blue shift of the Gr/AgNW/Gr sample is generated by the decreased Fermi velocity [24], which may correspond to the change in twist angle and layer separation between the two graphene layers induced by the AgNW network.

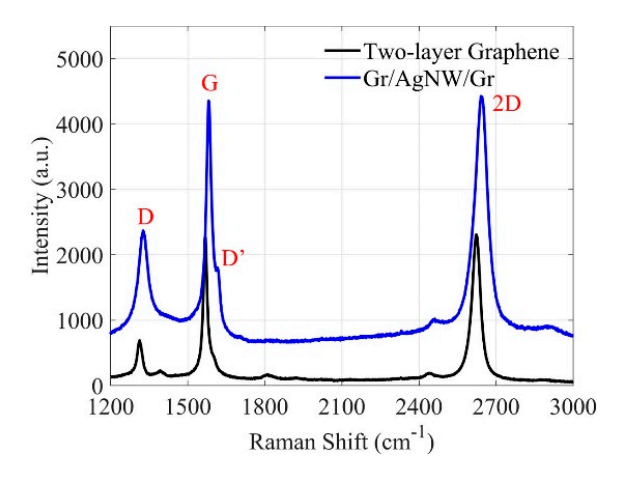


Figure 12. Raman spectra of two-layer graphene and the Gr/AgNW/Gr composite.

Table 4. Comparison of the peak values in Raman spectra of two-layer graphene and the composite.

| Sample | D-Peak (cm ⁻¹) | G-Peak (cm ⁻¹) | D'-Peak (cm ⁻¹) | 2D-Peak (cm ⁻¹) | I_G/I_{2D} |
|--------------|----------------------------|----------------------------|-----------------------------|-----------------------------|--------------|
| Two-layer Gr | 1319 | 1573 | NA | 2629 | 0.93 |
| Gr/AgNW/Gr | 1327 | 1582 | 1615 | 2642 | 0.98 |

3.6. Normalized Results

To summarize the results more clearly, the optical transmittance, sheet resistance, and stiffness values are normalized with the value of two-layer graphene set to 1. Figure 13 and Table 5 show the normalized values of the optical transmittance, sheet resistance, and stiffness, respectively. From 0.2 to 1.0 mg/mL of AgNW concentration increasing, the optical transmittance and sheet resistance reduce to 79% and 16% of the original two-layer graphene value, respectively. The stiffness of the composite increases at first and then becomes stable after 0.6 mg/mL with a value of approximately 4.6 times higher than two-layer graphene.

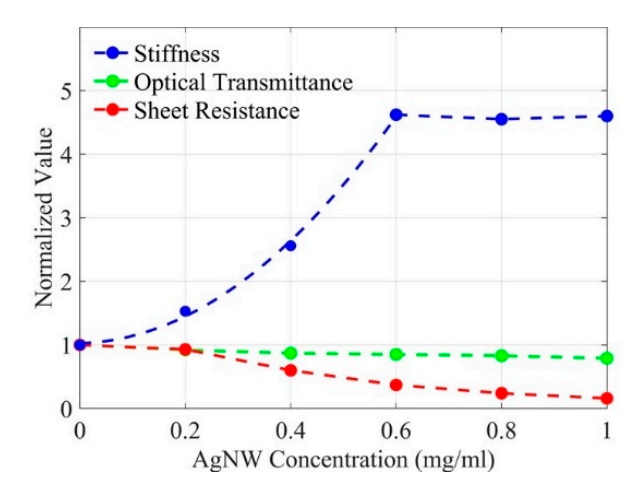


Figure 13. Normalized results of the stiffness, optical transmittance, and sheet resistance.

Appl. Sci. 2020, 10, 4802 11 of 12

| concentrations. | | | |
|-----------------------------|--------------------------|-----------------------------|-----------------|
| AgNW Concentrations (mg/mL) | Optical Transmittance | Sheet Resistance (Ω) | Stiffness (N/m) |
| 0 | 1 | 1 | 1 |
| 0.2 | 0.92 | 0.93 | 1 53 |

0.60

0.37

0.24

0.16

2.56

4.62

4.55

4.60

0.87

0.85

0.83

0.79

Table 5. Summary of the normalized properties of the graphene and composite under different AgNW concentrations.

4. Conclusions

0.4

0.6

0.8

1.0

In summary, the free-stand Gr/AgNW/Gr nanocomposite was synthesized through the LPCVD and vacuum annealing process for the first time in this work. Average spacing of the AgNW network, optical transmittance, sheet resistance, and stiffness of the nanocomposite were characterized under various AgNW concentrations. The characterization results can be used for transparent conductive film design based on specific parameter requirements. The stiffness results can be utilized for the interfacial bonding study between the AgNW and the Gr layer in the future.

Author Contributions: Conceptualization, C.G.; methodology, C.G., Y.L., and Y.Z.; writing—original draft preparation, C.G., Y.L., and Y.Z.; writing—review and editing, C.G., C.W. and G.C.; All authors have read and agreed to the published version of the manuscript.

Funding: This research was funded by the U.S. Department of Transportation, Office of the Assistant Secretary for Research and Technology (USDOT/OST-R), grant number 69A3551747126, through the INSPIRE University Transportation Center at Missouri University of Science and Technology. The views, opinions, findings, and conclusions reflected in this publication are solely those of the authors and do not represent the official policy or position of the USDOT/OST-R, or any State or other entity.

Acknowledgments: The author would like to thank to R. Brow in Missouri University of Science and Technology for getting the Raman Spectroscopy data.

Conflicts of Interest: The authors declare no conflict of interest.

References

- 1. Novoselov, K.S.; Geim, A.K.; Morozov, S.V.; Jiang, D.; Katsnelson, M.I.; Grigorieva, I.; Dubonos, S.; Firsov, A.A. Two-dimensional gas of massless Dirac fermions in graphene. *Nature* **2005**, *438*, 197. [CrossRef] [PubMed]
- 2. Geim, A.K. Graphene: Status and prospects. Science 2009, 324, 1530–1534. [CrossRef] [PubMed]
- 3. Kim, C.-L.; Jung, C.-W.; Oh, Y.-J.; Kim, D.-E. A highly flexible transparent conductive electrode based on nanomaterials. *NPG Asia Mater.* **2017**, *9*, 438. [CrossRef]
- 4. Ferrari, G.A.; De Oliveira, A.B.; Silvestre, I.; Matos, M.J.S.; Batista, R.J.C.; Fernandes, T.F.D.; Meireles, L.M.; Eliel, G.S.N.; Chacham, H.; Neves, B.R.A.; et al. Apparent Softening of Wet Graphene Membranes on a Microfluidic Platform. *ACS Nano* 2018, 12, 4312–4320. [CrossRef] [PubMed]
- 5. Stanford, M.G.; Li, J.T.; Chyan, Y.; Wang, Z.; Wang, W.; Tour, J.M. Laser-Induced Graphene Triboelectric Nanogenerators. *ACS Nano* **2019**, *13*, 7166–7174. [CrossRef] [PubMed]
- 6. Guo, C.; Fan, L.; Wu, C.; Chen, G.; Li, W. Ultrasensitive LPFG corrosion sensor with Fe-C coating electroplated on a Gr/AgNW film. *Sens. Actuators B Chem.* **2019**, *283*, 334–342. [CrossRef]
- 7. Guo, C.; Fan, L.; Chen, G. Corrosion-Induced Mass Loss Measurement under Strain Conditions through Gr/AgNW-Based, Fe-C Coated LPFG Sensors. *Sensors* **2020**, 20, 1598. [CrossRef]
- 8. Guo, W.; Wu, B.; Wang, S.; Liu, Y. Controlling Fundamental Fluctuations for Reproducible Growth of Large Single-Crystal Graphene. *ACS Nano* **2018**, *12*, 1778–1784. [CrossRef]
- 9. Li, X.; Cai, W.; Jung, I.; An, J.; Yang, D.; Velamakanni, A.; Piner, R.; Colombo, L.; Duoff, R.S. Synthesis, Characterization, and Properties of Large-Area Graphene Films. *ECS Trans.* **2009**, *19*, 41–52. [CrossRef]

Appl. Sci. 2020, 10, 4802 12 of 12

10. Seo, D.H.; Pineda, S.; Fang, J.; Gozukara, Y.; Yick, S.; Bendavid, A.; Lam, S.K.H.; Murdock, A.T.; Murphy, A.B.; Han, Z.J.; et al. Single-step ambient-air synthesis of graphene from renewable precursors as electrochemical genosensor. *Nat. Commun.* **2017**, *8*, 1–9. [CrossRef]

- 11. Chen, Z.; Qi, Y.; Chen, X.; Zhang, Y.; Liu, Z. Direct CVD Growth of Graphene on Traditional Glass: Methods and Mechanisms. *Adv. Mater.* **2019**, *31*, 1803639. [CrossRef] [PubMed]
- 12. Xie, Y.; Cheng, T.; Liu, C.; Chen, K.; Cheng, Y.; Chen, Z.; Qiu, L.; Cui, G.; Yu, Y.; Cui, L.; et al. Ultrafast Catalyst-Free Graphene Growth on Glass Assisted by Local Fluorine Supply. *ACS Nano* **2019**, *13*, 10272–10278. [CrossRef] [PubMed]
- 13. Mattevi, C.; Kim, H.; Chhowalla, M. A review of chemical vapour deposition of graphene on copper. *J. Mater. Chem.* **2011**, 21, 3324–3334. [CrossRef]
- 14. Kotakoski, J.; Meyer, J.C. Mechanical properties of polycrystalline graphene based on a realistic atomistic model. *Phys. Rev. B* **2012**, *85*, 195447. [CrossRef]
- 15. Kim, K.S.; Zhao, Y.; Jang, H.; Lee, S.Y.; Kim, J.M.; Kim, K.S.; Ahn, J.H.; Kim, P.; Choi, J.Y.; Hong, B.H. Large-scale pattern growth of graphene films for stretchable transparent electrodes. *Nature* **2009**, 457, 706–710. [CrossRef] [PubMed]
- 16. Suk, J.W.; Kitt, A.; Magnuson, C.W.; Hao, Y.; Ahmed, S.; An, J.; Swan, A.K.; Goldberg, B.B.; Ruoff, R.S. Transfer of CVD-grown monolayer graphene onto arbitrary substrates. *ACS Nano* **2011**, *5*, 6916–6924. [CrossRef] [PubMed]
- 17. Sun, J.; Deng, S.; Guo, W.; Zhan, Z.; Deng, J.; Xu, C.; Fan, X.; Xu, K.; Guo, W.; Huang, Y.; et al. Electrochemical bubbling transfer of graphene using a polymer support with encapsulated air gap as permeation stopping layer. *J. Nanomater.* **2016**, 2016. [CrossRef]
- 18. Lee, D.; Lee, H.; Ahn, Y.; Lee, Y. High-performance flexible transparent conductive film based on graphene/AgNW/graphene sandwich structure. *Carbon* **2015**, *81*, 439–446. [CrossRef]
- 19. Hu, L.; Kim, H.S.; Lee, J.; Peumans, P.; Cui, Y. Scalable Coating and Properties of transparent Ag nanowire. *ACS Nano* **2010**, *4*, 2955–2963. [CrossRef]
- Cho, S.; Kang, S.; Pandya, A.; Shanker, R.; Khan, Z.; Lee, Y.; Park, J.; Craig, S.L.; Ko, H. Large-Area Cross-Aligned Silver Nanowire Electrodes for Flexible, Transparent, and Force-Sensitive Mechanochromic Touch Screens. ACS Nano 2017, 11, 4346–4357. [CrossRef]
- 21. Kim, K.K.; Reina, A.; Shi, Y.; Park, H.; Li, L.J.; Lee, Y.H.; Kong, J. Enhancing the conductivity of transparent graphene films via doping. *Nanotechnology* **2010**, *21*. [CrossRef] [PubMed]
- 22. Ferrari, A.C.; Meyer, J.C.; Scardaci, V.; Casiraghi, C.; Lazzeri, M.; Mauri, F.; Piscanec, S.; Jiang, D.; Novoselov, K.S.; Roth, S. Raman spectrum of graphene and graphene layers. *Phys. Rev. Lett.* **2006**, 97, 187401. [CrossRef] [PubMed]
- 23. Dresselhaus, M.S.; Jorio, A.; Hofmann, M.; Dresselhaus, G.; Saito, R. Perspectives on carbon nanotubes and graphene Raman spectroscopy. *Nano Lett.* **2010**, *10*, 751–758. [CrossRef] [PubMed]
- 24. Ni, Z.; Wang, Y.; Yu, T.; You, Y.; Shen, Z. Reduction of Fermi velocity in folded graphene observed by resonance Raman spectroscopy. *Phys. Rev. B* **2008**, *77*, 235403. [CrossRef]



© 2020 by the authors. Licensee MDPI, Basel, Switzerland. This article is an open access article distributed under the terms and conditions of the Creative Commons Attribution (CC BY) license (http://creativecommons.org/licenses/by/4.0/).